Turbulence Modeling of Flowfields with Massive Surface Ablation

R.N. Gupta*
NASA Langley Research Center, Hampton, Virginia

A turbulence model accounting for the various physical phenomena in the viscous shock layer of a massively blown spherically blunted probe has been developed. In particular, an allowance has been made in the turbulence model for the longitudinal and normal pressure gradient effects, peaked massive ablation, and the nonequilibrium turbulence effects. The need for finding a boundary-layer edge is avoided. A computational mesh and convergence criterion more appropriate for the blown surface is employed in obtaining the results which include the effect of surface roughness.

Nomenclature

A^+ = measure of effective sublayer thickness
a_D = coefficient for production (enlargement) of mixing length
a_S = coefficient for dissipation (diminution) of mixing length
c^* = constant in Sutherland's law of viscosity, = 96.67 K for hydrogen
C_{KLEB} = constant in Klebanoff intermittency factor
H = nondimensional total enthalpy, H^*/u_∞^{*2}
i = finite-difference point in s direction
j = finite-difference point in n direction
k = kinetic energy of fluctuations; also time-step counter
l = mixing length given by Eq. (13)
$\bar{l}$ = mixing length given by Eq. (16)
$\bar{l}_r$ = mixing length given by Eq. (27)
M_∞ = freestream Mach number
M^* = molecular weight of mixture
$\dot{m}$ = surface injection rate, $\rho_w v_w/\rho_\infty u_\infty$
$\dot{m}_0$ = surface injection rate at the axis of symmetry
n = coordinate normal to the body, n^*/r_N^*
n^+ = normal coordinate
P^+ = pressure gradient parameter
Pr = Prandtl number
Pr_T = turbulent Prandtl number
p = nondimensional pressure, $p^*/\rho_\infty^* u_\infty^{*2}$
R^* = universal gas constant, J kg^{-1} K^{-1}
Re = freestream Reynolds number, $\rho_\infty^* u_\infty^* r_N^*/\mu_\infty^*$
R_g^* = gas constant, J kg^{-1} K^{-1}
Ri = Richardson number, $(2u^*/r_{eff}^*)/(\partial u^*/\partial n^*)_{av}$
R_h = nondimensional roughness height, R_h^*/r_N^*
r_{eff} = effective radius of curvature, $(r_N^*+n^*)/r_N^*$
r_N^* = nose radius, m
s = coordinate measured along the body, s^*/r_N^*
T = nondimensional temperature, T^*/T_∞^*
T_∞^* = freestream temperature, K
t = nondimensional time, $t^* U_\infty^*/r_N^*$
u = nondimensional tangential velocity, u^*/u_∞^*
u_∞^* = freestream velocity, ms^{-1}
u_τ = friction velocity
v = nondimensional normal velocity, v^*/u_∞^*
y = transformed coordinate along body surface
$\bar{y}$ = transformed coordinate given by Eq. (8)
z = transformed coordinate normal to body
$\bar{z}$ = transformed coordinate given by Eq. (8)
$\bar{z}_0$ = location where $(\partial H/\partial n)_{max}$ occurs
α = constant in mixing-length correction
β = pressure gradient parameter, $(\delta_i^*/\tau^*)(\partial p_w^*/\partial s^*)$
β_1, β_2 = stretching factors in Eq. (11)
γ = ratio of specific heats
$\gamma_{i,n}$ = Klebanoff normal intermittency factor
δ = shock standoff distance, δ^*/r_N^*
δ_i = incompressible displacement thickness, $\int_0^{\delta^*}(1-u^*/u_s^*)\,dn^*/r_N^* \neq \delta_i^*/r_N^*$
ϵ = a small number specified for convergence
ϵ^+ = normalized eddy viscosity, μ_T/μ
ζ = dimensionless total strain rate, $\zeta^* r_N^*/u_\infty^*$
κ = local curvature, $\kappa^* r_N^*$
μ = nondimensional viscosity, μ^*/μ_∞^*
μ_T = nondimensional eddy viscosity, μ_T^*/μ_∞^*
μ_∞^* = freestream viscosity, N s m^{-2}
ω = absolute vorticity of the flowfield
ρ = nondimensional density, ρ^*/ρ_∞^*
ρ_∞^* = freestream density, kg m^{-3}
σ = Reynolds number parameter, $(\mu_\infty^*/\rho_\infty u_\infty^* r_N^*)^{1/2}$
τ = transformed time given by Eq. (5)
$\bar{\tau}$ = transformed time given by Eq. (8)
$\bar{\tau}$ = local shear stress, $\tau^*/\rho_\infty u_\infty^{*2}$
θ_1, θ_2 = stretching parameters in Eq. (11)

Superscripts

( )* = dimensional quantity
k = time-step count
( )′ = fluctuating component

Subscripts

av = average
e = boundary-layer edge
i = inner law
o = outer law
mp = match-point
s = shock
w = wall
∞ = freestream

Presented as Paper 82-0198 at the AIAA 20th Aerospace Sciences Meeting, Orlando, Fla., Jan. 11-14, 1982; submitted Oct. 7, 1982; revision received March 31, 1983. This paper is declared a work of the U.S. Government and therefore is in the public domain.

*NRC-Senior Research Associate, Aerothermodynamics Branch, Space Systems Division. Member AIAA.

Introduction

TURBULENCE is one of the most important physical events in the flowfield of a blunt probe traveling at hypervelocity speeds under massive ablation conditions, and it plays a vital role in heat shield design considerations for such a probe. Recent studies[1] have demonstrated the large

penalty encountered due to the adverse effect that turbulence has on the ability of the injected ablation species to block or absorb radiation. Due to the severe entry conditions, the experimental simulation of such flowfields is very difficult if not impossible. There are some experimental data with massive blowing available in the literature.[2-5] They all suffer however, from the fact that they have been obtained for the freestream Mach number range of 3 to 7. The Jovian entry conditions are almost an order of magnitude more severe than the conditions employed in these experiments. Furthermore, Refs. 2-5 give mostly the surface convective heating results.† Not much information can be obtained about the flowfield structure from the surface convective heating under massive blowing conditions. The convective heating will be predicted to be negligible under these conditions by using almost any turbulence model! There are some detailed flowfield measurements reported[6] under moderate blowing conditions. Unfortunately, these measurements were also made at $M_\infty = 2.6$ only. The entrainment rate and turbulent mixing at these Mach numbers would be substantially different than those occurring during the Jovian entry conditions.[7] Therefore, this data base also cannot be relied upon for any better understanding of the flowfield for the purpose of turbulence modeling.

In the absence of a good experimenal data base against which a turbulence model can be verified, the theoretical design calculations should incorporate as much physics of the various events in the flowfield as possible. In particular, the turbulence model employed for the heat load calculations should be based on a good understanding of the various factors affecting the flowfield without requiring an excessive amount of computational time.

A typical probe shape designed to explore the atmosphere of outer planets would be a spherically blunted cone. Such a probe will have a high rate of mass injection from its ablative heat shield into the flow. The shock layer, contained between the shock and the probe, is expected to be turbulent over almost the entire length of the probe due to the massive ablation and large Reynolds number of the flow. The viscous shock layer for this flow situation would be characterized by an almost inviscid inner layer (close to the surface), a shear layer blown away from the surface, and an outer inviscid layer as shown in Fig. 1. The blown-off shear layer in this case does not quite behave as a free shear layer such as that encountered in a jet exhausting into a freestream. Over the spherical portion of the probe, the blown-off shear layer curves around the surface and retains a "memory" of the presence of a bounding surface. Also, the presence of the shock on the other side does not allow the shear layer to spread as freely as it would if it were truly a free shear layer unbounded by the surface as well as the shock wave. Therefore, in order to model such effects as those due to the surface curvature and roughness under massive blowing conditions, one should not ignore the presence of the wall since it is the source of these effects. However, the presence of the wall does not damp turbulence in this case the same way as it does in the case of no blowing.

Figure 4 of Ref. 2 (with helium injection and the blowing rate parameter = 1.05) clearly shows the convection of the small-scale eddies (generated near the surface) to outer regions of the flow due to massive blowing. The velocity near the surface is predominantly normal and the tangential velocity as well as its normal gradients are small. These observations are also supported by the velocity profiles obtained in the present work. Neither the gradients of the normal nor the tangential velocity near the surface are large enough to sustain any large amount of "turbulence" there, as evidenced

†For Jupiter entry, radiation is the dominant heat-transfer mechanism with the turbulent convective component normally less than 10% of the radiative component for peak heating conditions.

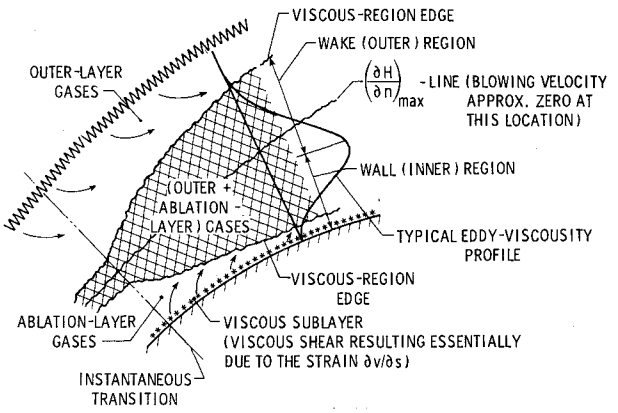

Fig. 1 Schematic of the flowfield around a re-entry probe with massive ablation.

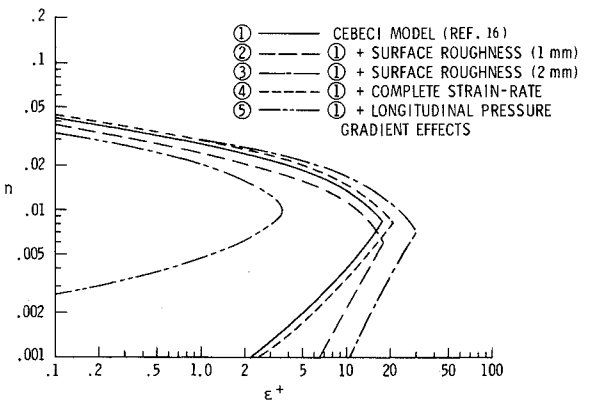

Fig. 2 Effect of various physical parameters on the eddy-viscosity profiles for $\dot{m}_o = 0.2$ and $s = 0.393$.

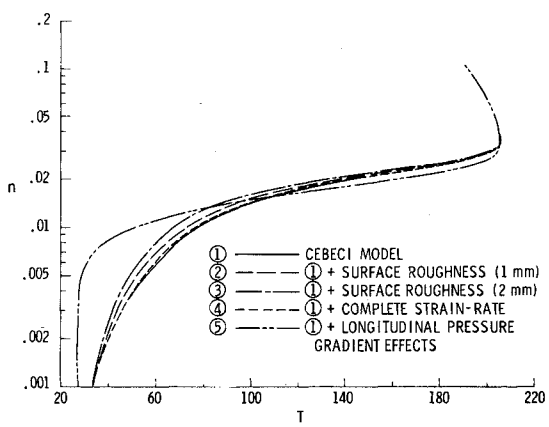

Fig. 3 Effect of various physical parameters in the turbulence model on temperature profiles for $\dot{m}_o = 0.2$ and $s = 0.393$.

by small values of the eddy viscosity. This conforms with the basic physics of the flow outlined earlier, namely, the presence of an almost inviscid flow between the blown layer and the wall. With this physical picture in mind, we may now be able to model the effect of various parameters on turbulent transport.

As indicated earlier, in the absence of a good data base for the Jovian entry conditions, any effort to make the turbulence model more complex would be meaningless. For such situations, one would like to draw upon the existing turbulence models and modify them by incorporating as much physics of the problem as possible. Since the Cebeci model[8] is the most widely used model for wall-bounded flows and as it is supported by Stanford's detailed[9] measurements under

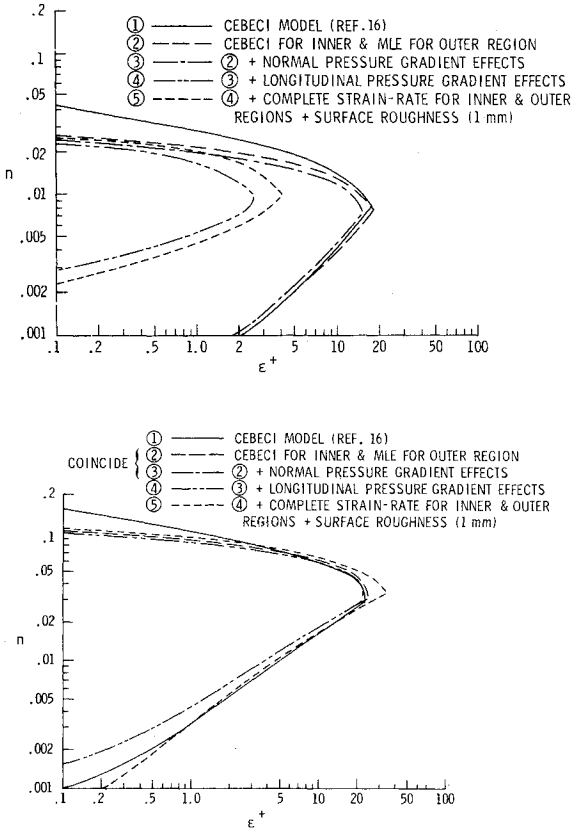

Fig. 4 Effect of the variation in turbulence model and physical parameters on eddy-viscosity profiles for $\dot{m}_0 = 0.2$: a) $s = 0.393$, spherical portion; b) $s = 1.767$, conical portion.

small surface mass transfer conditions for compressible flows, we have drawn heavily from this model in formulating the present two-layer eddy-viscosity model.

To account for the various factors influencing the flowfield, we have chosen a mixing-length formulation for the inner as well as outer region of the viscous-shock-layer flow, which is based on the complete strain rate. The longitudinal surface curvature effects have been accounted for essentially by following the approach of Refs. 10 and 11. The effect of longitudinal pressure gradient is included in the damping factor and Prandtl constant appearing in the Van Driest proposal for mixing length near the wall. The friction velocity near the wall has also been suitably modified through the integration of the momentum equation with massive surface blowing in the limit of normal distance shrinking to zero. Because of the difficulty of finding the boundary-layer edge for a radiating shock layer, the present model incorporates the modification that avoids such a necessity. Furthermore, growth of the large eddies in the outer layer with the streamwise distance has been accounted for by incorporating a simplified form of the length-scale equation.[12] Due to massive ablation, the nonequilibrium turbulence effects become important over the flank portion of the probe. These effects may not be important over the curved portion of the body since the large-scale eddies in the outer flow are suppressed there by the action of the normal pressure gradient. It is felt that the use of only the length-scale equation in preference to the more complex two-equation model of turbulence should be adequate to allow for the nonequilibrium effects for the problem under consideration. Unless the values of the various constants needed in the two-equation model are obtained from the appropriate experiments, it is sometimes not worth the extra effort, especially for the present case. The values of most of these constants employed in the earlier works[13] have been obtained from the experiments for subsonic flows.

It may now be summarized that the turbulence model outlined here adequately accounts for the vital physical events in the shock layer and can easily be combined with the viscous-shock-layer equations without substantially increasing the computational time. This criterion may be important for computing the flowfields with real-gas effects where the computations of radiative heating consume a substantial amount of computer time. Simplicity of the two-layer eddy-viscosity model and the ease with which it can be combined with the viscous-shock-layer equations have also played a major role in the formulation of the present model.

The turbulence model described herein has been combined with the conservative form of the time-dependent viscous-shock-layer equations. These equations are advanced in time to a steady state using the unsplit explicit finite-difference algorithm of MacCormack.[14] As pointed out earlier, the shear layer is blown away from the surface with massive blowing; therefore, the nodal spacing of the computational mesh should be more refined through the shear layer and not necessarily near the wall. In the present work, the refinement (i.e., compression) of the computational mesh is done in the region where the gradient of the total enthalpy is maximum. This approximately coincides with the location where the velocity normal to the surface becomes zero. However, since the magnitude of the normal velocity is very small and may vary in magnitude from iteration to iteration due to the computer roundoff errors even in the vicinity of converged solutions, it may not be meaningful to tie the mesh to the location where the stream function based on mass flux becomes zero, as suggested recently by some investigators.[15]

Analysis

Governing Equations

The flowfield solutions presented here were obtained by solving the conservative form of the time-dependent viscous-shock-layer equations for a perfect gas appropriate for both laminar and turbulent flow. These equations, when represented in the body-oriented coordinate system and for flow at zero angle of attack, are expressed as[1]

$$\frac{\partial U}{\partial t} + \frac{\partial M}{\partial s} + \frac{\partial N}{\partial n} + Q = 0 \tag{1}$$

where the vectors U, M, N, and Q may be obtained by dropping the species continuity equation and taking the mass fraction of species and radiative heat flux as zero in Eq. (1) of Ref. 1.

The following limiting form of the governing equations is obtained at the axis of symmetry (where $\beta = 0$) by differentiating Eq. (1) with respect to s and taking a limit as $s \to 0$:

$$\frac{\partial U_0}{\partial t} + \frac{\partial M_0}{\partial s} + \frac{\partial N_0}{\partial n} + Q_0 = 0 \tag{2}$$

where the vectors U_0, M_0, N_0, and Q_0 may once again be obtained from Eq. (2) of Ref. 1.

The equation of state is given by

$$p = [R^* T^*_\infty / M^* U^{*2}_\infty]\rho T \tag{3}$$

and the viscosity is obtained from Sutherland's law

$$\mu = [(1 + c^*/T^*_\infty)/(T + c^*/T^*_\infty)]T^{3/2} \tag{4}$$

Transformation to Computational Planes

The first of the two independent transformations employed maps the physical domain into a rectangular region in which both the shock and the body are made boundary mesh lines of the computational region. This transformation is

$$y \equiv s, \qquad z = 1 - n/\delta, \qquad \tau \equiv t \tag{5}$$

The transformed forms of Eqs. (1) and (2) are

$$\frac{\partial \bar{U}}{\partial \tau}+\frac{\partial \bar{M}}{\partial y}+\frac{\partial \bar{N}}{\partial z}+\bar{Q}=0 \tag{6}$$

$$\frac{\partial \bar{U}_0}{\partial t}+\frac{\partial \bar{M}_0}{\partial y}+\frac{\partial \bar{N}_0}{\partial z}+\bar{Q}_0=0 \tag{7}$$

where

$$\bar{U}=\delta U, \quad \bar{M}=\delta M, \quad \bar{N}=(1-z)(\delta_\tau U+\delta_y M)-N$$

$$Q=\delta Q, \qquad \delta_y=\partial\delta/\partial y, \qquad \delta_\tau=\partial\delta/\partial\tau$$

and

$$\bar{U}_0=\delta U_0, \qquad \bar{M}_0=\delta M_0$$

$$\bar{N}_0=(1-z)(\delta_\tau U_0+\delta_y M_0)-N_0, \qquad \bar{Q}_0=\delta Q_0$$

The computation region is then mapped to another plane to allow higher resolution through the shear layer which has been blown away from the surface due to massive blowing. The second transformation is

$$\bar{y}\equiv y, \qquad \bar{z}=f(z), \qquad \bar{\tau}\equiv\tau \tag{8}$$

With this transformation, the final forms of Eqs. (6) and (7) become

$$\frac{\partial \tilde{U}}{\partial \bar{\tau}}+\frac{\partial \tilde{M}}{\partial \bar{y}}+\frac{\partial \tilde{N}}{\partial \bar{z}}+\tilde{Q}=0 \tag{9}$$

$$\frac{\partial \tilde{U}_0}{\partial \bar{\tau}}+\frac{\partial \tilde{M}_0}{\partial \bar{y}}+\frac{\partial \tilde{N}_0}{\partial \bar{z}}+\tilde{Q}_0=0 \tag{10}$$

where

$$\tilde{U}\equiv\bar{U}, \qquad \tilde{M}\equiv\bar{M}$$

$$\tilde{N}=(1/F)\,[(1-z)(\delta_{\bar{\tau}}U+\delta_{\bar{y}}M)-N]$$

$$\tilde{Q}=\bar{Q}+(1/F^2)(\partial F/\partial\bar{z})\,[(1-z)(\delta_{\bar{u}}+\delta_{\bar{y}}M)-N]$$

and

$$\tilde{U}_0\equiv\bar{U}_0, \qquad \tilde{M}_0\equiv\bar{M}_0$$

$$\tilde{N}_0=(1/F)\,[(1-z)(\delta_{\bar{\tau}}U_0+\delta_{\bar{y}}M_0)-N_0]$$

$$\tilde{Q}_0=\bar{Q}_0+(1/F^2)(\partial F/\partial Z)\,[(1-z)(\partial_{\bar{\tau}}U_0+\partial_{\bar{y}}M_0)-N_0]$$

Here

$$z=\frac{1}{2}\left[\bar{z}_0\left\{\frac{\sinh(\beta_2\bar{z}-\theta_2)}{\sinh\theta_2}+1\right\}+\beta_1\frac{(\theta_1^{\bar{z}}-1)}{(\theta_1^{\bar{z}}+1)}\right]$$

$$F=\frac{1}{2}\left[\beta_2\bar{z}_0\frac{\cosh(\beta_2\bar{z}-\theta_2)}{\sinh\theta_2}+2\beta_1\ell n\theta_1\frac{\theta_1^{\bar{z}}}{(\theta_1^{\bar{z}}+1)^3}\right] \tag{11}$$

with

$$\frac{\partial F}{\partial\bar{z}}=\frac{1}{2}\left[\beta_2^2\bar{z}_0\frac{\sinh(\beta_2\bar{z}-\theta_2)}{\sinh\theta_2}+2\beta_1\theta_i^{\bar{z}}(\ell n\theta_1)^2\frac{(1-\theta_1^{\bar{z}})}{(\theta_1^{\bar{z}}+1)^3}\right]$$

$$\theta_1=(\beta_1+1)/(\beta_1-1); \qquad \theta_2=\ell n\left[\frac{1+(e^{\beta_2}-1)\bar{z}_0}{1+(e^{-\beta_2}-1)\bar{z}_0}\right]^{1/2}$$

The partial derivative with respect to n in the expressions for U, M, N, and Q is to be replaced by

$$\frac{\partial(\ )}{\partial n}=-\frac{1}{\delta}\frac{1}{F}\frac{\partial(\ )}{\partial\bar{z}}$$

Equation (11) refines the grid near $\bar{z}=\bar{z}_0$ and $\bar{z}=1$, while making the grid coarser at $\bar{z}=0$. Here $\bar{z}_0$ is the value of $\bar{z}$ where $(\partial H/\partial n)_{\max}$ or $[-(1/\delta)(1/F)\partial H/\partial\bar{z}]_{\max}$ occurs. This permits better solution of flowfield details near $\bar{z}_0$ and the body surface ($\bar{z}=1$). β_1 controls the amount of refinement near the surface, whereas β_2 provides control of the grid near $\bar{z}_0$. The practical value of β_1 ranges between 1 and 2 with values near 1 giving the largest amount of refinement. The practical range for β_2 is between 2 and 10 with a larger value providing the best resolution near z_0. Typical values of β_1 and β_2 employed in the computations were 1.2 and 4, respectively.

Boundary Conditions

The boundary conditions at the shock are calculated by using the Rankine-Hugoniot relations. At the body surface (wall), no velocity slip and no temperature jump are assumed. The surface blowing-rate distribution of Ref. 16 has been used and the surface temperature is taken as a prescribed value. Flow properties along the outflow boundary, where the main flow must be supersonic, are computed by extrapolation from the upstream grid points. Alternatively, they may also be obtained by using two-point backward differencing in both the predictor and corrector steps for computing the streamwise or tangential derivative.

Turbulence Model

A two-layer (inner and outer) eddy-viscosity/mixing-length formulation modified for nonequilibrium pressure gradient and longitudinal curvature effects and with allowances for peaked surface injection-rate distribution and surface roughness effects is presented here. Further, the necessity for finding the boundary-layer edge is also avoided. The inner eddy-viscosity model is used from the wall to the match-point (mp), where the eddy viscosity given by the inner model is equal to that of the outer model.

The dimensionless eddy viscosity is expressed in time-averaged fluctuating components as

$$\epsilon^+=\mu_T/\mu=-\overline{(\rho v)'u'}/\sigma^2\mu(\partial u/\partial n) \tag{12}$$

where the Reynolds-stress term $-\overline{(\rho v)'u'}$ is defined in terms of a mixing-length correlation as

$$-\overline{(\rho v)'u'}=\rho l^2|\zeta|(\partial u/\partial n) \tag{13}$$

Here ζ is the total strain-rate of the flowfield to account for the peaked surface injection rate distribution and is expressed as

$$\zeta=\frac{1}{(n+n\kappa)}\frac{\partial v}{\partial s}-\frac{1}{(1+n\kappa)}u+\frac{\partial u}{\partial n} \tag{14}$$

From Eqs. (12) and (13), the Prandtl's mixing-length concept may be stated as:

$$\epsilon^+=[\rho l^2/\sigma^2\mu]\,|\zeta| \tag{15}$$

Effect of Longitudinal Curvature on Mixing Length

Longitudinal streamline curvature has been shown[9,10] to affect the mixing length, l, for computational schemes using mixing-length/eddy-viscosity turbulence modeling. Accordingly, a formulation suggested by Bradshaw[11] is used herein to correct the mixing length for the effects of

longitudinal curvature and is given by

$$l=\bar{l}(1-\alpha Ri) \tag{16}$$

where $\alpha=3$ and $\alpha Ri<0.7$ in the outer portion of the viscous region over the curved portion. This limiting value of Ri in the outer region is justified in view of the experiments of Ref. 17. These experiments give a value of $\bar{l}=0.025\delta$ over the curved portion, compared to a value of $\bar{l}=0.085\delta$ over the flat portion. Further, the value of $(\partial u/\partial n)_{av}$ employed in obtaining the Richardson number, Ri, is an average taken over all the grid points from the match-point (mp) to the shock-wave location:

$$\left(\frac{\partial u}{\partial n}\right)_{av}=\sum_{N=N_{mp}}^{N_s}\left(\frac{\partial u}{\partial n}\right)_N \Big/ \sum_{N=N_{mp}}^{N_s} 1$$

Now, over the spherical portion of a blunted body,

$$r_{eff}=l+n \tag{17}$$

and a lag equation is used to smooth out abrupt changes in curvature:

$$\mathrm{d}(1/r_{eff})/\mathrm{d}s=-1/(10n_{max}r_{eff}) \tag{18}$$

Here n_{max} is the value of n at which F_{max}, defined by,[18]

$$F(n)=n\omega \tag{19}$$

occurs and ω is the absolute magnitude of vorticity given as

$$\omega=\left|\frac{1}{1+\kappa n}\frac{\partial v}{\partial s}-\frac{\partial u}{\partial n}-\frac{\kappa}{1+\kappa n}u\right| \tag{20}$$

Inner Eddy-Viscosity Formulation

The eddy viscosity for the inner region of the viscous layer is obtained from Eq. (15) rewritten as:

$$\epsilon_i^+=\frac{\rho\bar{l}^2(1-\alpha Ri)^2}{\sigma^2\mu}|\zeta| \tag{15a}$$

to allow for the longitudinal curvature effects introduced through Eq. (16). The mixing length, $\bar{l}$, is evaluated by using the Van Driest's[8] proposal stated as

$$\bar{l}=Kn[1-\exp(-n^+/A^+)] \tag{21}$$

where

$$n^+=\frac{n\rho}{\sigma\mu}\left\{\left|\frac{\tilde{\tau}}{\rho}\right|\right\}^{1/2}=\frac{n\rho}{\sigma\mu}\left\{\left|\left[\mu_w\left(\frac{\partial u}{\partial n}\right)_w+\rho_w v_w u+\frac{\partial p_w}{\partial s}n\right]\Big/\rho\right|\right\}^{1/2}$$

In defining n^+, $\tilde{\tau}$ has been used in place of τ_w to allow for the effect of blowing on the mixing length in a direct way. There is negligible convective acceleration near the wall, so that

$$\tilde{\tau}=\mu_w\left(\frac{\partial u}{\partial n}\right)_w+\dot{m}u+\frac{\partial p_w}{\partial s}n \tag{22}$$

Under the massive blowing conditions, typical values of n^+/A^+ in Eq. (21) are of the order of 10^6 over the spherical portion of the probe. For such a situation, Eq. (21) yields

$$\bar{l}=Kn \tag{21a}$$

Thus, the damping influence of the wall is automatically removed from Eq. (21) when the blowing is massive. Further, depending on the value of $\partial v/\partial s$ (required to sustain turbulence near the wall), eddy viscosity is predicted appropriately from Eq. (15a) with the inclusion of total strain rate ζ.

Thus, the basic concept of the Prandtl-Van Driest-Cebeci formulation employed for the inner layer here seems to give the correct physics for the flowfield under massive blowing conditions. This physics is further reflected from the velocity profiles obtained in the present work.

Effect of Pressure Gradient on A^+

The effective sublayer thickness A^+ is strongly affected by local pressure gradients and was modeled based on Ref. 19. The experimenal data of Ref. 19 cover the range of approximately $-0.07<p^+<0.07$, where p^+ is the pressure gradient parameter

$$p^+=[\sigma^2\mu/\rho^2u_\tau^3](\partial p/\partial s)_w \tag{23}$$

For $p^+<-0.07$, the value of A^+ was held constant at the value obtained for $P^+=-0.07$. Thus, the sublayer thickness employed for flows with a pressure gradient is:

$$A^+=26(1+11.8P^+)^{-1/2} \text{ for } P^+>-0.03$$

$$=26(1-11.8\times 0.03)^{-1/2} \text{ for } P^+<-0.03 \tag{24a}$$

and for flows with both a pressure gradient and massive injection ($\rho_w v_w>0.1$):

$$A^+=26\left\{\frac{P^+}{v^+}[\exp(11.8v^+)-1]+\exp(11.8v^+)\right\}^{-1/2}$$

for $P^+\geq -0.07$

$$=26\left\{-\frac{0.07}{v^+}[\exp(11.8v^+)-1]+\exp(11.8v^+)\right\}^{-1/2}$$

for $P^+<-0.07$ (24b)

where $v^+=v_w/u_\tau$ and

$$u_\tau=\sigma\left\{\left|\frac{\tilde{\tau}}{\rho}\right|\right\}^{1/2}=\sigma\left\{\left|\left[\mu_w\left(\frac{\partial u}{\partial n}\right)_w+\rho_w v_w u+\frac{\partial p_w}{\partial s}n\right]\Big/\rho\right|\right\}^{1/2}$$

With moderate surface injection rates, bounds on A^+ for larger values of the favorable pressure gradients may be obtained from the experimental results contained in Ref. 19.

Effect of Pressure Gradient on Prandtl Constant (K)

The effect of the longitudinal pressure gradient on the value of the slope of the mixing length near the wall, K, has been accounted for through the relation between K and the pressure gradient parameter β defined as:

$$\beta=\frac{1}{\sigma^2}\left\{\delta_i\Big/\left[\mu_w\left(\frac{\partial u}{\partial n}\right)_w+\rho_w v_w u+\left(\frac{\partial p_w}{\partial s}\right)n\right]\right\}\frac{\partial p_w}{\partial s} \tag{25}$$

where δ_i is the incompressible displacement thickness.

The variation of K with β used in the analysis is[20]

$$K=0.44+0.182[1-\exp(0.321\beta)] \text{ for } \beta>0$$

$$=0.004(\beta+10)^2 \text{ for } -10<\beta<0 \tag{26}$$

For values of β less than -10, K may be assumed to be zero (laminarized condition).

Effect of Surface Roughness

The mixing length in Eq. (21) may be modified to include the influence of surface roughness by following the approach of Ref. 21. Thus, for a rough surface, the mixing length, $\bar{l}$, in

Eq. (21) is obtained from:

$$\bar{l}_r = K(n+\Delta n)\left[1-\exp\left(-\frac{n^+ + \Delta n^+)}{A^+}\right)\right] \tag{27}$$

with n^+ and A^+ as defined earlier and

$$\Delta n^+ = 0.9[\sqrt{R_h^+} - R_h^+ \exp(-R_h^+/6)]$$

$$R_h^+ = \frac{R_h \rho}{\mu\sigma}\left\{\left|\left[\mu_w\left(\frac{\partial u}{\partial n}\right)_w + \rho_w v_w u + \frac{\partial p_w}{\partial s} n\right]\Big/\rho\right|\right\}^{1/2}$$

$$\Delta n = (n/n^+)\Delta n^+; \qquad R_h = R_h^*/r_N^*$$

Outer Eddy-Viscosity Approximation

For the outer region of the visous layer also, the eddy viscosity is obtained from Eq. (15) by combining it with the Klebanoff intermittency fator. Thus,

$$\epsilon_o^+ = \frac{\rho \bar{l}(1-\alpha Ri)^2}{\sigma^2 \mu}\,|\zeta|\gamma_{i,n} \tag{15b}$$

where the mixing length has been modified for the longitudinal curvature effects with the help of Eq. (16) and $\gamma_{i,n}$ is the Klebanoff intermittency factor defined as

$$\gamma_{i,n} = [1+5.5(C_{\text{KLEB}} n/n_{\max})^6]^{-1} \tag{28}$$

In Eq. (28) $n_{\max}$ is the value of n where $F(n)$, defined by Eq. (19), is maximum.[18] The constant C_{KLEB} was found to be unity by requiring agreement with the results of Ref. 8.

Since the flow in the outer region of a massively blown shock layer resembles to some exent the free-mixing layers, a length-scale equation should describe the growth of the mixing length with streamwise distance. The length-scale equation suggested by Spalding[12] is

$$u_{\text{av}}(s)\frac{\mathrm{d}\bar{l}}{\mathrm{d}s} = a_D k^{1/2} - a_S(\bar{\tau}/\rho)^2 k^{-3/2} \tag{29}$$

In the outer portion of the viscous region, convection makes a significant contribution and an appropriate balance may be taken to exist between the convective term and the production term resulting from the enlargement of $\bar{l}$ in Eq. (29).

$$u_{\text{av}}(s)\frac{\mathrm{d}\bar{l}}{\mathrm{d}s} = a_D k^{1/2} \tag{30}$$

Here u_{av} is the average velocity across the wake region and may be taken as

$$u_{\text{av}} = (u_s + u_{mp})/2 \tag{31}$$

where u_s is the velocity behind the shock and u_{mp} is the velocity where $\epsilon_i^+ = \epsilon_o^+$. It would appear more appropriate to use the velocity at the edge of viscous layer u_e in place of u_s in Eq. (31), as pointed out in Ref. 22. Due to the difficulty of finding the boundary-layer edge for a radiating shock layer, however, it is proposed to use u_s in place of u_e. This results in a somewhat larger value of $\bar{l}$ and, consequently, ϵ_o^+. The increase in ϵ_o^+ is offset, possibly through the use of a larger value (1 rather than 0.3) for C_{KLEB} in Eq. (28). Now, kinetic energy of the turbulent fluctuations, k, may be obtained from[23]

$$k^{1/2} = 0.3\,|u_s - u_{\text{mp}}| \tag{32}$$

Using a value[12] of 0.27 for the coefficient a_D in Eq. (30) and combining it with Eq. (32) gives:

$$u_{\text{av}}\frac{\mathrm{d}\bar{l}}{\mathrm{d}s} = 0.081\,|u_s - u_{\text{mp}}| \tag{33}$$

The constant appearing in Eq. (33) is based on low-speed data and is more appropriate for unconfined free-mixing flows. In the absence of any better experimental data for the Jovian entry conditions, the only other way to find the value of this constant would be to use Eq. (33) for the small blowing case and tune in the value of the constant by comparing it with the Cebeci model predictions. This procedure results in a somewhat lower value of the constant, and Eq. (33) is modified to

$$u_{\text{av}}\frac{\mathrm{d}\bar{l}}{\mathrm{d}s} = 0.005\,|u_s - u_{mp}| \tag{34}$$

The smaller value of the constant in Eq. (34), which actually represents the spread rate of the viscous layer in the outer portion of the shock layer, appears more appropriate for application to the viscous-shock-layer type of flows since Spalding's coefficients were meant primarily for flow situations without the confining effect of a shock wave. It may also be pointed out here that the value of the constant appearing in Eq. (34) might require some further modification in view of the results obtained recently.[24] However, any effort to make the turbulence model more complex would be meaningless until we have a good data base for the Jupiter entry conditions.

Finally, Eq. (34) upon integration yields the mixing length $\bar{l}$ to be used with Eq. (15b):

$$\bar{l}(s) = 0.01\int_{s=0}^{s} \frac{|u_s - u_{\text{mp}}|}{(u_s + u_{\text{mp}})}\,\mathrm{d}s \tag{35}$$

An equation similar to Eq. (34) has also been obtained in Ref. 25 through a somewhat different procedure.

Method of Solution

A time-asymptotic two-step finite-difference method due to MacCormack[14] is used to solve the governing equations. A forward-predictor backward-corrector operator sequence is used for each time step in the vectorized code[26] ideally suited for the CDC Cyber 203 computer. In the present analysis, the eddy viscosity and new grid are obtained after every 25 time steps to save computing time.

Discussion of Results

As pointed out in the introduction, this study was undertaken primarily to account for the various physical events in modeling turbulence for the massively blown viscous shock layers. In addition, a computational mesh and convergence criterion more appropriate for such flowfields and surface roughness effects were included in the analysis.

The solutions presented here were obtained using 101 grid points normal to the body with a variable grid spacing, whereas those along the body were evenly spaced at Δs values of 0.1963 through $s = 2.7482$. For all the solutions obtained, the transition to turbulent flow was instantaneous and located at the first body grid downstream of the stagnation point.

The flow conditions used in the analysis are those of Ref. 16, considered typical of the Jovian entry conditions at that time. Although the probe shape, mass, and other entry conditions have changed since then, the case of Ref. 16 was retained for the present study to allow comparisons with the published results.

Probe geometry: 45 deg half-angle spherically blunted cone with a nose radius (r_N^*) of 0.22 m.

Jovian atmosphere: Hydrogen-helium mixture (0.90 H_2 + 0.10 He) under perfect-gas conditions.

Other flowfield parameters: $M_\infty = 43.84$; $T_\infty^* = 145$ K; $\rho_\infty^* = 1.27\times10^{-4}$ kg m^{-3}; $T_w^* = 4000$ K, $\gamma = 1.224$; $R_g^* = 3593.6$ J kg^{-1} K^{-1}; $Re = 156{,}700$; $Pr = 0.72$; $\dot{m}_0 = 0.2$; the surface blowing-rate distribution of Ref. 16 is employed.

In the present analysis, the result is considered as converged to the steady-state value when the following criterion is

satisfied:

$$\text{maximum}_{i,j} \left| \left[(\partial H/\partial n)^k - (\partial H/\partial n)^{k-500} \right] / (\partial H/\partial n)^k_{i=1} \right| < \epsilon$$

where $\epsilon \approx 0$ (10^{-3}). This test is made after every 500 time steps.

In the results presented here, first the effects of surface roughness, complete strain rate, and the longitudinal pressure gradient considered separately with the Cebeci model of turbulence are given in Figs. 2 and 3. The cumulative effect of these variations on the proposed eddy-viscosity model employing a mixing-length formulation in the inner as well as outer region is presented in Figs. 4-6. With this formulation, the effects of longitudinal surface curvature and nonequilibrium turbulence have also been accounted for. Finally, Fig. 7 gives results for no surface injection and Fig. 8 presents the Richardson number distribution (associated with surface curvature).

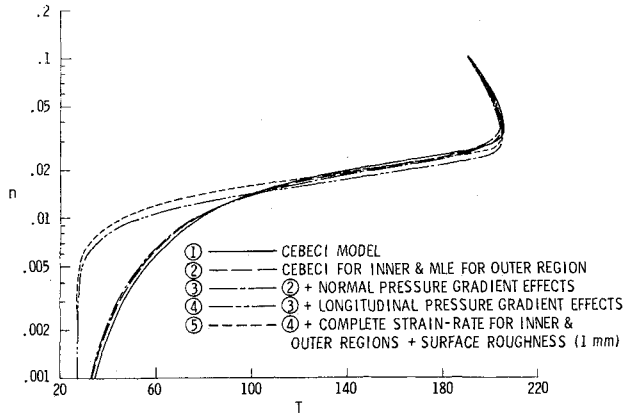

Fig. 5 Effect of the variation in turbulence model and physical parameters on temperature profiles for $\dot{m}_0 = 0.2$ and $s = 0.393$.

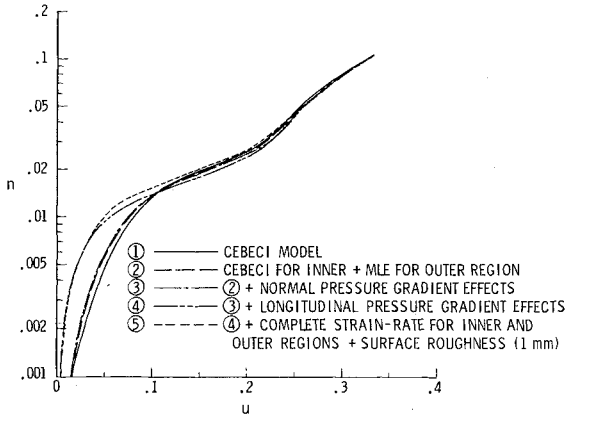

Fig. 6 Effect of the variation in turbulence model and physical parameters on tangential velocity profiles for $\dot{m}_0 = 0.2$ and $s = 0.393$.

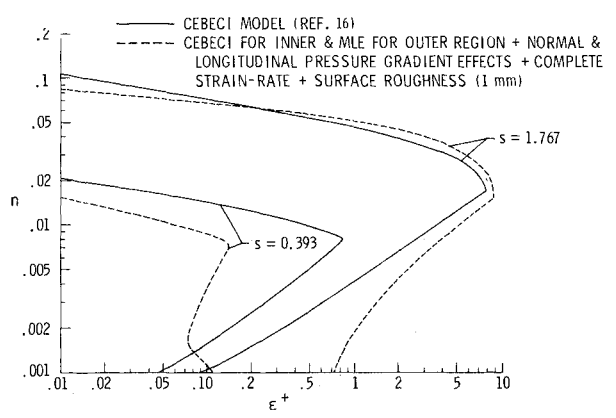

Fig. 7 Effect of the variation in turbulence model and physical parameters on eddy-viscosity profiles for $\dot{m}_0 = 0$.

Figure 2 contains the eddy-viscosity profiles obtained by including the effects of surface roughness, total strain rate, and the longitudinal pressure gradient in the Cebeci turbulence model of Ref. 8. The results of Ref. 16, which do not include these effects, are also shown for comparison. As expected, surface roughness increases eddy viscosity as compared to a smooth surface of Ref. 16. This effect is more noticeable when the surface-roughness height is increased from 1 to 2 mm. With the stronger surface blowing, however, the surface may appear "smooth" to the blown shock layer. Furthermore, care must be taken in choosing the step size near the wall such that the first grid point away from the wall is located at a distance of the order of Δn, defined in Eq. (27). Otherwise, the effect of surface roughness will be smeared out near the wall. The inclusion of complete strain-rate also increases the eddy viscosity but to a somewhat lesser degree as compared to the surface roughness. The effect of longitudinal pressure gradient on eddy-viscosity distribution, however, is much more noticeable over the spherical portion (as shown in Fig. 2 for $s = 0.393$) where the gradient is strongly favorable. Over the conical flank portion, the various effects are of the same order of magnitude. For the sake of brevity, these results are not included here. The temperature profiles corresponding to the various cases of Fig. 2 are contained in Fig. 3. With the suppression of turbulence by the longitudinal pressure gradient, the upper edge of the blown viscous layer is somewhat lower, implying lesser entrainment of the high-temperature outer region gases. Further, a smaller value of the eddy viscosity would cause reduction in the transport of these hot gases to the lower region by turbulent diffusion. This would suggest lower temperatures closer to the surface as shown in Fig. 3.

Two of the main problems associated with the Cebeci turbulence model are that the normal pressure gradient effects (arising essentially from the longitudinal surface curvature) cannot be properly accounted for in a straightforward manner, and for a radiating viscous shock layer, it is difficult to find the viscous-layer edge. For the massively blown case the additional inadequacy of the Cebeci model is reflected from the fact that eddy viscosity in the outer region is computed as a local property, whereas the flowfield is highly nonsimilar or is in a nonequilibrium state. Figure 4 shows the results obtained by employing a mixing-length equation (MLE), Eq. (35), for the outer region eddy-viscosity calculations. With the formulation contained in Eqs. (15b), (28) and (35), the objections mentioned here have been taken care of. Once again, Fig. 4 also contains the eddy-viscosity

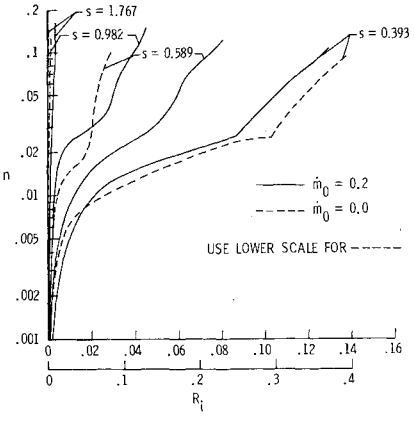

Fig. 8 Richardson number distribution corresponding to curve ⑤ of Fig. 4 for $\dot{m}_0 = 0.0$ and $\dot{m}_0 = 0.2$.

profile of Ref. 16 obtained by the basic Cebeci turbulence model of Ref. 8. The role played by the normal pressure gradient in reducing the length scale of large eddies which carry the upstream history is clearly brought out for the outer region over the curved portion of the probe (Fig. 4a). The inclusion of longitudinal pressure gradient effects suppresses turbulence closer to the surface as before. Figure 4 also shows a curve which has the combined effect of normal and longitudinal pressure gradient, complete strain rate, and surface roughness. The net result is an overall reduction of eddy viscosity and also lowering of the upper edge of the blown viscous layer. The smaller temperatures in the lower region and less-full velocity profile due to poor turbulent diffusion as shown in Figs. 5 and 6, respectively, for this case are consistent.

Figure 7 shows the eddy-viscosity profiles obtained with the complete model of Fig. 4 (shown as curve (5)) for the case of no surface blowing. Overall results are similar to those for the massively blown case. However, the surface roughness seems dominant now in controlling the eddy viscosity, especially over the conical portion of the probe. Over the curved portion, the reduction in eddy viscosity by the action of normal and logitudinal pressure gradients is still substantial. Closer to the surface, the surface-roughness effects appear to take over unlike the blown case.

Figure 8 shows the role played by the normal pressure gradient in reducing the large eddy structure in the outer region and the recovery of the flowfield from curved to the flat surface as measured through Richardson number distribution. Massive blowing appears to reduce the normal pressure gradient and its ability to destroy the outer eddies, thereby making the flow more nonequilibrium. Finally, with the adoption of the new grid, the computational time has been reduced by about 25% as compared with the computations of Ref. 16 employing a logarithmic grid for the same order of accuracy. This saving results from the avoidance of excessive grid refinement near the surface for a massively blown flowfield.

Concluding Remarks

The flowfield solutions for a massively blown surface are presented with a turbulence model, which accounts for the normal and longitudinal pressure gradients, surface roughness, and nonequilibrium character of the flow. The need for finding the boundary-layer edge is also avoided. Further, a computational mesh and the convergence criterion more appropriate for the blown surface are employed. There is a net reduction of turbulent mixing and lowering of the viscous-layer edge with the accounting of these various effects. The reduction is more noticeable over the curved portion. This has the implication of suggesting a lower penalty resulting from the adverse effect of turbulence on an ablating surface. With the new computational grid suggested here, the computational time for the massively blown viscous shock layers has been found to be lower by about 25% as compared with those employing a logarithmic-grid distribution for the same degree of accuracy.

Acknowledgments

The author wishes to acknowledge many helpful suggestions offered by J.J. Jones, D.M. Bushnell, Dr. J.N. Moss, and Dr. A. Kumar of NASA Langley.

References

[1] Moss, J.N. and Kumar, A., "Significance of Turbulence and Transition Location on Radiative Heating with Ablation Injection," AIAA Paper 81-0281, St. Louis, Mo., Jan. 1981.

[2] Kattari, G.E., "The Effect of Simulated Ablation-Gas Injection on the Shock Layer of Blunt Bodies at Mach Numbers of 3 and 5," NASA TN D-2954, 1965.

[3] Feldhuhn, R.H., "Heat Transfer from a Turbulent Boundary Layer on a Porous Hemisphere," AIAA Paper 76-119, Washington, D.C., Jan. 1976.

[4] Demetriades, A., Laderman, A.J., and Von Seggern, L., "Effect of Mass Addition on the Boundary Layer of a Hemisphere at Mach 6," *Journal of Spacecraft and Rockets,* Vol. 13, Aug. 1976, pp. 508-509.

[5] Kattari, G.E., "Effects of Mass Addition on Blunt Body Boundary-Layer Transition and Heat Transfer," NASA TP 1139, Sept. 1977.

[6] Fernandez, F.L. and Zukoski, E.E., "Experiments in Supersonic Turbulent Flow with Large Distributed Surface Injection," *AIAA Journal,* Vol. 7, Sept. 1969, pp. 1759-1766.

[7] Gupta, R.N., "Parameters for the Simulation of High Temperature Blown Shock Layers," *AIAA Journal,* Vol. 21, Feb. 1983, pp. 314-316.

[8] Cebeci, T., "Behavior of Turbulent Flow Near a Porous Wall with Pressure Gradient," *AIAA Journal,* Vol. 8, Dec. 1970, pp. 2152-2156.

[9] Kays, W.M. and Moffat, R.J., "The Behavior of Transpired Turbulent Boundary Layers," *Studies in Convection, Vol. 1: Theory, Measurement and Application,* Academic Press, London, 1975.

[10] Simon, T.W., Moffat, R.J., Johnston, J.P., and Kays, W.M., "Turbulent Boundary Layer Heat Transfer Experiments: Convex Curvature Effects, Including Introduction and Recovery," Rept. HMT-32, Mech. Eng., Stanford University, Nov. 1980.

[11] Bradshaw, P., "Effects of Streamline Curvature on Turbulent Flow," AGARDograph No. 169, Aug. 1973.

[12] Spalding, D.B., "The Calculation of the Length Scale of Turbulence in Some Turbulent Boundary Layers Remote From Walls," Rept. TWF/TN/31, Dept. of Mech. Eng., Imperial College, London, Sept. 1967.

[13] Gupta, R.N. and Wakelyn, N.T., "Theoretical Study of Reactive and Nonreactive Turbulent Coaxial Jets," NASA TN D-8127, Aug. 1976.

[14] MacCormack, R.W., "The Effect of Viscosity in Hypervelocity Impact Cratering," AIAA Paper 69-354, Cincinnati, Ohio, April 1969.

[15] Menees, G.P. and Lombard, C.L., "The Effect of Modeled Turbulence on a Hypersonic Shock Layer with Massive Ablation Injection," AIAA Paper 81-1071, Palo Alto, Calif., June 1981.

[16] Kumar, A., Graves, R.A., Jr., and Tiwari, S.N., "Laminar and Turbulent Flows Over a Spherically Blunted Cone with Massive Surface Blowing," *AIAA Journal,* Vol. 17, Dec. 1979, pp. 1326-1331.

[17] Gillis, J.C., Johnston, J.P., Moffat, R.J., and Kays, W.M., "Experimental Data and Model for the Turbulent Boundary Layer on a Convex, Curved Surface," NASA CR-3391, March 1981, pp. 95-105.

[18] Baldwin, B.S. and Lomax, H., "Thin Layer Approximation and Algebraic Model for Separated Turbulent Flows," AIAA Paper 78-257, Huntsville, Ala., Jan. 1978.

[19] Crawford, M.E. and Kays, W.M., "STAN5—A Program for Numerical Computation of Two-Dimensional Internal and External Boundary Layer Flows," NASA CR-2742, Dec. 1976.

[20] Cary, A.M. Jr., Weinstein, L.M., and Bushnell, D.M., "Drag Reduction Characteristics of Small Amplitude Rigid Surface Waves," in *AIAA Progress in Astronautics and Aeronautics,* Vol. 72, edited by G.R. Hough, New York, 1980, pp. 144-167.

[21] Cebeci, T. and Chang, K.C., "Calculation of Incompressible Rough-Wall Boundary-Layer Flows," *AIAA Journal,* Vol. 16, July 1978, pp. 730-735.

[22] Gupta, R.N., Moss, J.N., Zoby, E.V., and Simmonds, A.L., "An Evaluation of Turbulence Models for Massively Blown Surfaces," AIAA Paper 83-0875, St. Louis, Mo., June 1982; also to appear in the AIAA Progress Series, 1983.

[23] Schetz, J.A., "Injection and Mixing in Turbulent Flow," *AIAA Progress in Astronautics and Aeronautics,* Vol. 68, 1980.

[24] Gupta, R.N. and Moss, J.N., "Effect of Low-Reynolds-Number Turbulence Amplification on Galileo Probe Flowfield," *Journal of Spacecraft and Rockets,* Vol. 20, July-Aug. 1983, pp. 409-411.

[25] Nicolet, W.E. and Balakrishnan, A., "Methods for Predicting Off-Stagnation Point Flowfields for Planetary Entry Probes," AIAA Paper 79-1083, Orlando, Fla., June 1979.

[26] Kumar, A. and Graves, R.A., Jr., "A Vectorized Code for Calculating Laminar and Turbulent Hypersonic Flows About Blunt Axisymmetric Bodies at Zero and Small Angles of Attack," NASA TM 80202, Jan. 1980.